Streaming and removal forces due to second-order sound field during megasonic cleaning of silicon wafers

P. A. Deymier[a)]
Department of Materials Science and Engineering, University of Arizona, Tucson, Arizona 85721

J. O. Vasseur, A. Khelif, B. Djafari-Rouhani, and L. Dobrzynski
Laboratoire de Dynamique et Structure des Matériaux Moléculaires, UPRESA CNRS 8024, UFR de Physique, Université des Sciences et Technologies de Lille 59655 Villeneuve d'Ascq Cédex, France

S. Raghavan
Department of Materials Science and Engineering, University of Arizona, Tucson, Arizona 85721

(Received 20 March 2000; accepted for publication 13 September 2000)

We calculate the second-order streaming force in a fluid in the vicinity of the solid/fluid interface for two systems of importance in the technology of megasonic cleaning of silicon wafers. The first system consists of a single planar interface between a solid elastic medium representing silicon and a viscous fluid, namely water. The second system accounts for the finite thickness of silicon wafers. It is composed of one silicon slab (wafer) immersed in water. The components of the streaming force parallel and normal to the silicon/water interface are determined as functions of frequency and wave vector of the incident acoustic wave. The normal component of the streaming force is used to calculate the removal force defined as the net force perpendicular to the solid/fluid interface acting on a spherical contaminant particle adhering to the silicon surface. The removal force is too small to remove submicron particles. In contrast the streaming force parallel to the solid/fluid interface may remove particles by pushing or rolling them. The streaming force is shown to be very sensitive to the angle the incident acoustic wave makes with the silicon/water interface. © *2000 American Institute of Physics.* [S0021-8979(00)05324-X]

I. INTRODUCTION

Megasonic waves have been extensively used to remove contaminant particles from silicon wafers during manufacturing of semiconductor devices. In this process, planar silicon wafers are immersed in a water-based solution and subjected to a beam of sonic energy with a frequency in the range 600 KHz–1 MHz. The acoustic wave propagates typically along directions parallel to the wafer/fluid interface. Much of the work in the area of megasonic cleaning has been directed towards finding conditions such as megasonic power and duration of field to optimize particle removal. Several processes are known or believed to be operative in a megasonic field, namely microcavitation, acoustic streaming, and pressure induced chemical effects. However, it has not been established to any reasonable degree of confidence whether these phenomena are responsible for particle removal. A brief review of the mechanisms that have been claimed to be responsible for the cleaning action in a megasonic field is pertinent at this stage.

The megasonic waves can be visualized as pressure variations propagating into the fluid at the speed of sound. When a sonic wave passes over a solid particle, the pressure gradient in that wave exerts a force acting on that particle.[1] Since the pressure front typically propagates parallel to the surface of the wafer, the acoustic force on an adsorbed particle is parallel to the wafer surface and should not be able to dislodge the particle by opposing the adhesion force. This force may only push the particle along the surface of the wafer. Olim[1] has shown that the acoustic pressure force on an isolated particle in water is proportional to the cube of the diameter of the particle. This author has then estimated that for particles with a diameter less than 0.35 μm, the pressure force is smaller than the adhesion force and that megasonic cleaning in absence of any other cleaning mechanism will not be efficient. Olim's model neither accounts for the interaction of the incident acoustic wave with the wafer nor its scattering by the contaminant particle. A more realistic model of the acoustic pressure field has been derived by Wu.[2] However, this model is limited to a single wafer immersed in a nonviscous fluid and was not used to determine the pressure force on deposited contaminant particles. We have recently calculated the acoustic pressure force due to scattering of a megasonic wave by a submicron particle deposited on a silicon substrate.[3] We have shown that scattering of the acoustic wave by deposited submicron particles is negligible and that the pressure field in the vicinity of the solid/fluid interface is primarily controlled by transmission and reflection. Since efficient particle removal is expected to result from processes that are associated with high energy densities, the scattering of an incident acoustic wave with millimeter wavelength by a submicron particle adhering at a wafer/water interface is unlikely to lead to a sufficient energy concentration.

Microcavitation is produced by the pressure variations in sound waves moving through the liquid. Cavitation bubbles

a)Electronic mail: deymier@oxygen.mse.arizona.edu

are formed by the low-pressure components of the acoustic wave. This component causes a hole or cavity to form in the liquid. This cavity implodes when the walls can no longer sustain the compressive forces. During cavitation, the formation of a cavity and its subsequent collapse is able to concentrate the low energy density of the sound wave into a very small volume leading locally to very high pressures and temperatures. The contaminant particles may serve as nucleation centers that cause the cavities to collapse before they can fully develop. The transfer of energy from the cavities to the particles may therefore dislodge the particles. Cavitation appears to be an important mechanism in ultrasonic cleaning. However, it had been claimed that in megasonic cleaning the time between megasonic pulses on the order of 1.25 μs is too short for the formation of cavities.[4] Following this argument, Shwartzman *et al.*[4] suggested that the cleaning action in megasonic cleaning resulted from rocking action due to high-pressure waves rather than cavitation. More recently, however, cavitation was detected in a megasonic tank by sonoluminescence.[5] These experimental measurements indicate that the maximum cavitation intensity occurs near the water surface of the megasonic tank. It may then be concluded from this observation that this cleaning mechanism should not result in effective particle removal since the transient cavitation activity is concentrated near the water surface and therefore will not affect most of the wafer area.[5] However, the presence of stable cavitation throughout the megasonic cleaning tank may probably assist cleaning efficiency by introducing microstreaming currents near the wafer surface.

The loss of acoustic momentum that results from attenuation or dissipation of the sound field in a viscous fluid may result in a time-independent fluid motion (stationary vortices), known as acoustic streaming.[6] When considering the acoustic field in a viscous medium, viscosity leads to time-independent second-order effects such as acoustic streaming. Acoustic streaming may be treated as a nonlinear correction to the linear (first-order) acoustic field. Acoustic streaming can occur either in a free nonuniform sound field or near obstacles immersed in the sound field. There are several types of acoustic streaming classified in terms of scale, namely Eckart's quartz-wind-like streaming,[7] Schlichting streaming in boundary layers[8] and microstreaming near secondary sound sources such as oscillating bubbles or vibrating particles on surfaces.[9]

The boundary conditions imposed on the acoustic field at the interface between a solid and a viscous fluid result in the fluid flow within a viscous boundary layer near the interface known as Schlichting streaming. Eckart streaming occurs outside the acoustic boundary layer. Eckart streaming is generated by a free nonuniform attenuated sound field that has the inhomogenity scale significantly larger than the acoustic wavelength. Microstreaming is another type of microscale streaming. It is associated with fluid vortices resulting from secondary sound sources such as sound waves scattered by oscillating bubbles in a viscous medium.

Megasonic cleaning efficiency is often improved when using a chemically active cleaning medium such as SC1 cleaning solutions. SC1 cleaning solutions are water-based solutions of hydrogen peroxide and ammonia. The ability of a megasonic field to induce interesting chemical effects has been reported.[10] In water containing nitrogen gas, application of a megasonic field has been shown to create $NH4^+$ and NO_3^- ions. In hydrogen peroxide solutions, hydroxyl radicals (OH) appear to form in the presence of a megasonic field. However, it is not known whether a megasonic field can enhance the dissolution materials such as SiO_2 through the formation of such species. The most commonly accepted mechanism for particle removal from Si surfaces using SC1 solutions is that the peroxide in the solution creates a thin oxide film which is then etched by ammonium hydroxide. Particles are presumed to be removed during the etching of the oxide. The etch rate of oxide in conventional SC1 solutions has been measured to be approximately 0.3 nm/min. In more dilute solutions, the etch rate may be expected to be even smaller and consequently the ''oxide etch'' theory for particle removal has come under some criticism. Since the use of megasonic energy in dilute SC1 solutions is effective in removing particles from wafer surfaces, it is possible that the etch rate of oxide is increased by the megasonic field.

The preceding brief review of the current understanding of some of the mechanisms that may be responsible for the cleaning action in megasonic tanks demonstrates a clear need for a more fundamental study of the megasonic cleaning process. Experimental studies of megasonic cleaning are clouded by the overlap of the possible mechanisms. The complexity of some of these mechanisms added to the very small spatial scales involved render the design of unambiguous experiments difficult. To date experimental investigations have not been able to pin point the exact mechanism of particle removal by megasonic waves and only empirical methods have allowed advancement in megasonic particle removal. We have therefore elected to undertake a theoretical study of the megasonic cleaning and in particular of some of the individual phenomena that are susceptible to removing contaminant particles from silicon wafers.

The primary objective of the present article is to investigate, theoretically, phenomena associated with second-order sound fields such as acoustic streaming and more, specifically Schlichting streaming on particle removal during megasonic cleaning. This theoretical study consists of two parts, namely the calculation of the time-dependent (first-order) acoustic displacement field at solid/viscous-fluid interfaces, followed by the calculation of the time-independent (second-order) pressure field.

The nonlinear motion in a viscous fluid is governed by the Navier–Stokes equation. For small velocities, Navier–Stokes equation can be linearized. This linearized equation for sound propagation in a fluid is completely analogous to that of elasticity theory for an isotropic solid where the longitudinal and transverse sound velocities are replaced by complex numbers. Solving for the acoustic field near a solid immersed in a viscous fluid requires a simultaneous treatment of the Navier–Stokes equation for the fluid and the elastic wave equation for the solid with appropriate boundary conditions at the interfaces. We use the method of the interface response theory (IRT) based on the formalism of Green's functions[11] to calculate the first-order acoustic dis-

placement field. The IRT provides an attractive framework for the calculation of acoustic properties of inhomogeneous media. The response function (e.g., acoustic Green's function) of an inhomogeneous medium (e.g., wafer in a fluid) can be calculated in terms of the known bulk Green's functions of each constitutive subsystem (wafer or fluid) and ''interface response operators'' which account for the geometry of the various interfaces. The Green's function formalism is then applied to the calculation of first-order velocity field due to scattering of an incident acoustic wave by: (1) a semi-infinite solid/viscous-fluid interface (i.e., a semi-infinite elastic solid in contact along its surface with a semi-infinite viscous fluid); (2) a wafer immersed in a viscous fluid modelled as a slab of elastic solid sandwiched between two semi-infinite viscous fluid media.

For the calculation of second-order corrections to the sound field, a method developed by Nyborg[12] is used. Starting with the nonlinear Navier–Stokes equation, Nyborg makes the approximation that its solution is the superposition of first-order and second-order contributions to the displacement (or velocity) field. The first term varies sinusoidally in time with a frequency ω and thus represents the first-order sound field. The second-order term is time independent and may give rise to acoustic streaming. In Nyborg's approach, one begins by determining the first-order approximation to the velocity (this is the sound field calculated with the Green's function method), then one uses this in getting a second-order approximation. Nyborg defines the streaming force F in terms of the time average over several sonic cycles of gradients of the first-order velocity field. The streaming force F can then be interpreted as the time rate of increase of momentum in the fluid. It is equivalent to some external force field that, provided flow is not constrained, may be driving the fluid into streaming motion. If the fluid is constrained not to flow then the streaming force is balanced by the gradient of the second-order acoustic pressure.

This article is organized as follows. In Sec. II we introduce the methods and models with some details. Section III reports on the results for the streaming force obtained in the case of a single silicon/water interface and of a silicon slab (wafer) immersed in water. The removal force on a spherical contaminant particle resulting from the streaming force is calculated in Sec. IV. In this same section, we compare the removal force to the adhesion force that drives the particle toward the silicon surface. There we consider only the contribution of the van der Waals forces to adhesion. Several cases previously analyzed in Sec. III are studied. Finally, we draw some conclusions concerning the effect of the streaming force on particle removal in megasonic cleaning.

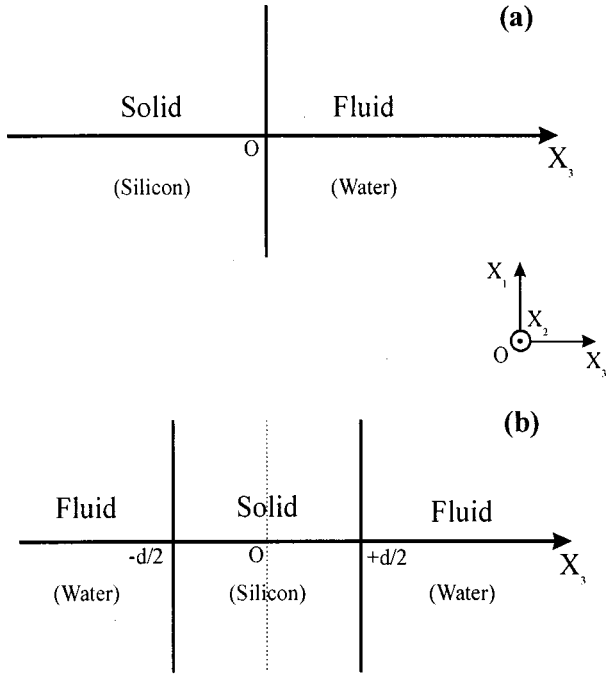

FIG. 1. Illustration of the two inhomogeneous systems studied, (a) the silicon/water system and (b) the water/silicon/water system.

II. MODELS AND METHOD

A. Models

In a typical megasonic cleaning tank, several wafers are cleaned at one time. The wafers are arranged parallel to each other in cassettes. The medium through which the megasonic waves propagate is inhomogeneous and may therefore be simply represented as a layered composite consisting of alternating silicon slabs separated by water-based fluid layers. Since wafer diameters are significantly larger than the wavelength of megasonic waves, the layered composite is treated here as being infinite in directions parallel to the wafer/fluid interfaces. Furthermore, for the sake of simplicity of the models we take the solid medium as being isotropic. In this article we consider two multilayer geometries. First, we investigate the interaction between an incident acoustic wave and a single interface between two semi-infinite homogeneous media composed of silicon and water, respectively. This system will be called the silicon/water system. This simple interface is used to establish the mathematical procedure for calculating the second-order sound field. A more realistic geometry corresponding to one wafer immersed in water is then treated. This system with two parallel interfaces is modeled as a solid slab of silicon separating two semi-infinite media of water. Since the radius of a silicon wafer exceeds by far its thickness, the slab is considered to be of infinite length. We will refer to that system as the water/silicon/water system.

Figure 1 illustrates the type of layered composite systems studied in this article. All interfaces are chosen to be perpendicular to the axis X_3 of a Cartesian coordinate system (X_1, X_2, X_3).

B. First-order (linear) equations of motion and Green's function formalism

In this subsection we formulate the equations necessary to describe motion in an elastic solid (silicon) and a viscous fluid (water). The equation of motion for the displacement u_α, $\alpha=1,2,3$ of a point in an infinite homogeneous three-dimensional elastic material is

$$\rho \ddot{u}_\alpha = \sum_\beta \frac{\partial \sigma_{\alpha\beta}}{\partial X_\beta}, \tag{1}$$

where ρ is the mass density, $\ddot{u}_\alpha$ the second derivative with respect to the time t of u_α and $\sigma_{\alpha\beta}$ the stress tensor

$$\sigma_{\alpha\beta} = \sum_{\mu\nu} C_{\alpha\beta\mu\nu}\eta_{\mu\nu}. \tag{2}$$

$C_{\alpha\beta\mu\nu}$ are the usual elastic constants and $\eta_{\mu\nu}$ the deformation tensor

$$\eta_{\mu\nu} = \frac{1}{2}\left(\frac{\partial u_\mu}{\partial X_\nu} + \frac{\partial u_\nu}{\partial X_\mu}\right). \tag{3}$$

With these definitions and assuming that the fluid excitations execute harmonic motion with pulsation ω ($\omega = 2\pi\nu$ where ν is the frequency) and a time dependence $e^{-i\omega t}$, the equation of motion (1) becomes

$$-\rho\omega^2 u_\alpha = \sum_{\beta\mu\nu} C_{\alpha\beta\mu\nu}\frac{\partial^2 u_\mu}{\partial X_\beta \partial X_\nu}. \tag{4}$$

For an isotropic elastic medium

$$C_{\alpha\beta\mu\nu} = C_{12}\delta_{\alpha\beta}\delta_{\mu\nu} + C_{44}(\delta_{\alpha\mu}\delta_{\beta\nu} + \delta_{\alpha\nu}\delta_{\beta\mu}) \tag{5}$$

with $C_{12} = C_{11} - 2C_{44}$. The symbol δ_{ij} is the Kroenecker symbol equal to 1 when $i = j$ and 0 when i is different from j. The longitudinal and transverse plane wave velocities, C_l and C_t, are given respectively by the relations

$$C_l^2 = \frac{C_{11}}{\rho} \quad \text{and} \quad C_t^2 = \frac{C_{44}}{\rho}. \tag{6}$$

If we introduce in Eq. (4) the operator

$$H_{\alpha\mu}(\boldsymbol{r}) = \rho\omega^2\delta_{\alpha\mu} + \sum_{\beta\nu} C_{\alpha\beta\mu\nu}\frac{\partial^2}{\partial X_\beta \partial X_\nu} \tag{7}$$

we may define the bulk response function (or Green's function), $G_{\mu\nu}(\boldsymbol{r},\boldsymbol{r}')$, as the solution of the equation

$$\sum_\mu H_{\alpha\mu}(\boldsymbol{r})G_{\mu\nu}(\boldsymbol{r},\boldsymbol{r}') = \delta_{\alpha\nu}\delta(\boldsymbol{r}-\boldsymbol{r}'). \tag{8}$$

Since one will later deal with inhomogeneous media separated by parallel interfaces, it is convenient to make a Fourier analysis of the Green's function parallel to a plane ($X_3 = 0$). We further apply a rotation of the X_1, X_2 axes that brings the X_1 axis along the wave vector $\boldsymbol{k}_\parallel$ parallel to the plane. After these transformations, Eq. (8) becomes

$$\rho\begin{pmatrix} \omega^2 - k_\parallel^2 C_l^2 + C_t^2\frac{d^2}{dX_3^2} & 0 & ik_\parallel(C_l^2 - C_t^2)\frac{d}{dX_3} \\ 0 & \omega^2 + C_t^2\left(\frac{d^2}{dX_3^2} - k_\parallel^2\right) & 0 \\ ik_\parallel(C_l^2 - C_t^2)\frac{d}{dX_3} & 0 & \omega^2 - k_\parallel^2 C_l^2 + C_t^2\frac{d^2}{dX_3^2} \end{pmatrix} \times \begin{pmatrix} G_{11} & G_{12} & G_{13} \\ G_{21} & G_{22} & G_{23} \\ G_{31} & G_{32} & G_{33} \end{pmatrix} = \delta(X_3 - X_3')\begin{pmatrix} 1 & 0 & 0 \\ 0 & 1 & 0 \\ 0 & 0 & 1 \end{pmatrix}. \tag{9}$$

In the preceding equation $G_{\mu\nu}$ stands for $G_{\mu\nu}(k_\parallel\omega|X_3, X_3')$. Let us recall that Eq. (9) leads to $G_{12} = G_{21} = G_{23} = G_{32} = 0$, that is a decoupling between sagittal and transverse polarizations.

The motion of the bulk fluid, in the absence of external forces, is governed by the Navier–Stokes equation

$$\rho\left[\frac{\partial \boldsymbol{v}}{\partial t} + (\boldsymbol{v}\cdot\nabla)\boldsymbol{v}\right] = -\nabla p + \mu\nabla^2\boldsymbol{v} + \left(\mu' + \frac{1}{3}\mu\right)\nabla(\nabla\cdot\boldsymbol{v}), \tag{10}$$

where $\boldsymbol{v}$ is the velocity, ρ the density, μ and μ' the coefficients of shear and dilatation viscosity, and p the pressure. For small velocities, Eq. (10) can be linearized after neglecting the term $(\boldsymbol{v}\cdot\nabla)\boldsymbol{v}$. Assuming, as in the case of the solid, that the fluid excitations execute harmonic motion with pulsation ω, the velocity $\boldsymbol{v}$ is related to the displacement $\boldsymbol{u}$ by

$$\boldsymbol{v} = -i\omega\boldsymbol{u}. \tag{11}$$

Finally, we assume that the pressure term in Eq. (10) is due only to the density fluctuations giving rise to dilatation and compression of the fluid. That is, we neglect the contribution due to thermal fluctuations. Then

$$p = -\lambda(\nabla\cdot\boldsymbol{u}), \tag{12}$$

where λ is the compressibility of the fluid which is related to the (longitudinal) sound velocity C via

$$C^2 = \frac{\lambda}{\rho}. \tag{13}$$

With the above assumptions, the stress tensor in the liquid can be written as

$$\sigma_{\alpha\beta} = \lambda(\nabla\cdot\boldsymbol{u})\delta_{\alpha\beta} + \mu\left[\frac{\partial v_\alpha}{\partial X_\beta} + \frac{\partial v_\beta}{\partial X_\alpha} - \frac{2}{3}\delta_{\alpha\beta}(\nabla\cdot\boldsymbol{v})\right] + \mu'\delta_{\alpha\beta}(\nabla\cdot\boldsymbol{v}). \tag{14}$$

This form of the stress tensor is completely analogous to that obtained in elasticity theory for an isotropic solid. The following correspondences should be made:

$$C_{l(f)}^2 = C^2 - \frac{i\omega}{\rho}\left(\mu' + \frac{4}{3}\mu\right),$$
$$C_{t(f)}^2 = -\frac{i\omega\mu}{\rho}, \tag{15}$$

where $C_{l(f)}$ and $C_{t(f)}$ are the fluid equivalent of the velocities of the longitudinal and transverse sound waves in a solid.

The derivation of the bulk Green's function of the viscous fluid can be done step by step along the same lines as for the isotropic solid. The Green's function of the fluid is therefore given by Eq. (9) provided the velocities of the sound waves are replaced by those given in Eq. (15). The Green's function of a bulk homogeneous elastic medium is reported in the appendix in the form of Eq. (A1).

C. Interface response theory

The IRT[11] allows for the construction of the Green's function of an inhomogeneous medium in terms of the Green's functions of the block constituents of the composite. The Green's function of a composite medium can be written in the form of an interface integral equation

$$\begin{aligned}\overleftrightarrow{g}(\mathbf{r},\mathbf{r}') = \overleftrightarrow{G}(\mathbf{r},\mathbf{r}') + \int d\mathbf{r}_M \overleftrightarrow{G}(\mathbf{r},\mathbf{r}_M) \int d\mathbf{r}'_M \overleftrightarrow{G}^{-1}(\mathbf{r}_M,\mathbf{r}'_M) \\ \times \int d\mathbf{r}''_M [\overleftrightarrow{g}(\mathbf{r}'_M,\mathbf{r}''_M) - \overleftrightarrow{G}(\mathbf{r}'_M,\mathbf{r}''_M)] \\ \times \int d\mathbf{r}'''_M \overleftrightarrow{G}^{-1}(\mathbf{r}''_M,\mathbf{r}'''_M)\overleftrightarrow{G}(\mathbf{r}'''_M,\mathbf{r}'), \\ \{\mathbf{r},\mathbf{r}'\} \in D, \quad \{\mathbf{r}_M,\mathbf{r}'_M,\mathbf{r}''_M,\mathbf{r}'''_M\} \in M \end{aligned} \tag{16}$$

with

$$\overleftrightarrow{G}(\mathbf{r},\mathbf{r}') = \begin{cases} \overleftrightarrow{G}_i(\mathbf{r},\mathbf{r}'), & \{\mathbf{r},\mathbf{r}'\} \in D_i, i = 1,N \\ 0 \quad \mathbf{r} \in D_i,\ \mathbf{r}' \in D_j, i \neq j, \end{cases} \tag{17}$$

where D represents the space of the entire inhomogeneous medium, M is the total domain of interfaces, and D_i is the space in which the constitutive block i is defined. In the case of layered composites media, using two-dimensional Fourier transforms of the Green's function in a plane parallel to the interfaces, the domain of the interfaces reduces to points along the X_3 axis, thus the integrals in Eq. (16) reduce to discrete sums over these points.

We note that in order to solve for $\overleftrightarrow{g}(\mathbf{r},\mathbf{r}')$ using Eq. (16), one needs to know its form in the domain of the interfaces, $\overleftrightarrow{g}(\mathbf{r}_M,\mathbf{r}''_M)$. According to the IRT, the inverse of the Green's function of the inhomogeneous medium defined in the domain of the interfaces may be expressed in terms of the inverse Green's function of the constitutive blocks defined in the domain of their surfaces, such that

$$\begin{aligned} &\overleftrightarrow{g}^{-1}(\mathbf{r} \in M_{ij}, \mathbf{r}' \in M_{kl}) = 0 \quad \text{if } M_{kl} \notin M_i, \\ &\overleftrightarrow{g}^{-1}(\mathbf{r} \in M_{ij}, \mathbf{r}' \in M_{il}) \\ &\quad = \overleftrightarrow{g}_s^{-1}(\mathbf{r} \in M_{ij}, \mathbf{r}' \in M_{il}) \quad \text{if } l \neq j, \\ &\overleftrightarrow{g}^{-1}(\mathbf{r} \in M_{ij}, \mathbf{r}' \in M_{ij}) \\ &\quad = \sum_k \overleftrightarrow{g}_s^{-1}(\mathbf{r} \in M_{kl}, \mathbf{r}' \in M_{kl}) \quad \text{if } M_{kl} \equiv M_{ij}, \end{aligned} \tag{18}$$

with M_{ij} standing for the interface between the constitutive blocks i and j. In Eq. (18) $\overleftrightarrow{g}_s$ stands for the Green's function of the constitutive blocks with free surfaces. All the boundary conditions (e.g., continuity of displacement) at the interfaces are satisfied through Eq. (18). The inhomogeneous media considered in this study are composed of semi-infinite media and slabs. The Green's function of a semi-infinite medium or a slab is obtained from the bulk Green's function defined previously. In the presence of a free surface or free surfaces, Eq. (9) has to be solved subject to the boundary conditions expressing the absence of stress at the surface. The inverse of the Green's function at the surface of a semi-infinite elastic medium and at the surfaces of an elastic slab have been reported in the literature and presented in the appendix.

In addition to the Green's function, the IRT allows for the determination of the elastic displacement field resulting from the scattering of an incident wave by the interfaces in the inhomogeneous medium. If $\boldsymbol{U}(\mathbf{r})$ represents a bulk incident wave launched in one homogeneous piece of the composite system, the displacement field, $\boldsymbol{u}(\mathbf{r})$, including all the waves reflected and transmitted by the interfaces is then given by the relation

$$\begin{aligned}\boldsymbol{u}(\mathbf{r}) = \boldsymbol{U}(\mathbf{r}) - \int d\mathbf{r}_M \overleftrightarrow{G}(\mathbf{r},\mathbf{r}_M) \int d\mathbf{r}'_M \overleftrightarrow{G}^{-1}(\mathbf{r}_M,\mathbf{r}'_M)\boldsymbol{U}(\mathbf{r}'_M) \\ + \int d\mathbf{r}_M \overleftrightarrow{G}(\mathbf{r},\mathbf{r}_M) \int d\mathbf{r}'_M \overleftrightarrow{G}^{-1}(\mathbf{r}_M,\mathbf{r}'_M) \\ \times \int d\mathbf{r}''_M \overleftrightarrow{g}(\mathbf{r}'_M,\mathbf{r}''_M) \int d\mathbf{r}'''_M \overleftrightarrow{G}^{-1}(\mathbf{r}''_M,\mathbf{r}'''_M) U(\mathbf{r}'''_M), \\ \{\mathbf{r},\mathbf{r}'\} \in D,\ \{\mathbf{r}_M,\mathbf{r}'_M,\mathbf{r}''_M,\mathbf{r}'''_M\} \in M \end{aligned} \tag{19}$$

with Eq. (17) still applying.

Finally, the total variation of the density of vibrational states $\Delta n(\omega)$ between the composite system and a reference system may be determined from the knowledge of $\overleftrightarrow{g}^{-1}$ in the space of the interfaces.[11] For layered composites it is convenient to use a matrix representation of the inverse of the Green's function in the space M, namely, $\overleftrightarrow{g}^{-1}(M,M)$. With such a notation, the total variation in density of states is given by

$$\begin{aligned}\Delta n(\omega) = -\frac{1}{\pi}\frac{d}{d\omega}(&\arg\det \overleftrightarrow{g}^{-1}(MM) \\ &- \arg\det \overleftrightarrow{g}_{\text{ref}}^{-1}(MM)), \end{aligned} \tag{20}$$

where ref stands for the reference system.

At this stage we have at hand the tools to characterize the first-order (time-dependent) acoustic field at an interface

between an isotropic elastic solid and a viscous fluid. In the next section we show following Nyborg[12] that this first-order sound field can be used to determine the time-independent second-order solution to the nonlinear Navier–Stokes equation.

D. Second-order (nonlinear) correction to sound field: Nyborg's method

To determine the time-independent second-order solution to the nonlinear Navier–Stokes equation, we use a method developed by Nyborg[12] to calculate second-order corrections to the acoustic field in a viscous fluid. Starting with the nonlinear Navier–Stokes equation, Nyborg makes the approximation that its solution is the superposition of a steady-state sound field and a steady flow. The velocity, pressure, and density fields are therefore written as

$$\begin{aligned} \boldsymbol{v} &= \boldsymbol{v}_1 + \boldsymbol{v}_2, \\ p &= p_0 + p_1 + p_2, \\ \rho &= \rho_0 + \rho_1 + \rho_2. \end{aligned} \tag{21}$$

Here, p_0 and ρ_0 are some static pressure and the density of the fluid in absence of acoustic field. $\boldsymbol{v}_1$, p_1, and ρ_1 are first-order approximations to solutions of the Navier–Stokes equation. These quantities vary sinusoidally in time with a pulsation ω and thus represent the sound field solution to the linearized form of the Navier–Stokes equation. The second-order terms, $\boldsymbol{v}_2$, p_2, and ρ_2, are time independent. The term $\boldsymbol{v}_2$ is the acoustic streaming velocity and describes a steady-state flow of the fluid. The acoustic streaming velocity may be obtained from an equation derived by Nyborg and accurate up to second order

$$\mu \nabla^2 \boldsymbol{v}_2 = \nabla p_2 - \boldsymbol{F}, \tag{22}$$

where $\boldsymbol{F}$ is an effective source force of streaming related to the first-order velocity $\boldsymbol{v}_1$ by

$$-\boldsymbol{F} \equiv \rho_0 \langle (\boldsymbol{v}_1 \cdot \nabla)\boldsymbol{v}_1 + \boldsymbol{v}_1(\nabla \cdot \boldsymbol{v}_1) \rangle. \tag{23}$$

The brackets $\langle\ \rangle$ indicate that a time average is taken over several sonic cycles. With Nyborg's approach, one begins by determining the first-order approximation to the velocity (this is the sound field calculated with the Green's function method or IRT), then one uses this in getting a second-order approximation.

Equation (23) can be simplified in the case of layered composites. We first recall that one can make a Fourier analysis of the displacement field parallel to the plane of the interfaces, namely the plane $X_3 = 0$. Provided that we have chosen the X_1, X_2 axes such that the two-dimensional wave-vector $\boldsymbol{k}_\parallel$ is parallel to X_1, the components of the first-order displacement field $\boldsymbol{u_1}$ take the form in complex notation

$$\begin{aligned} \tilde{u}_1(X_1,0,X_3,t) &= \tilde{u}_1(k_\parallel \omega | X_3) e^{ik_\parallel X_1} e^{-i\omega t}, \\ \tilde{u}_2(X_1,0,X_3,t) &= 0, \\ \tilde{u}_3(X_1,0,X_3,t) &= \tilde{u}_3(k_\parallel \omega | X_3) e^{ik_\parallel X_1} e^{-i\omega t}, \end{aligned} \tag{24}$$

with $\boldsymbol{u_1} = \mathrm{Re}\{\tilde{\boldsymbol{u}}_1\}$ where Re stands for the real part of the complex quantity $\tilde{\boldsymbol{u}}_1$.

The components of the first-order velocity $\boldsymbol{v_1}$, in complex notation, are therefore given by

$$\begin{aligned} \tilde{v}_1(X_1,0,X_3,t) &= -i\omega \tilde{u}_1(k_\parallel \omega | X_3) e^{ik_\parallel X_1} e^{-i\omega t}, \\ \tilde{v}_2(X_1,0,X_3,t) &= 0, \\ \tilde{v}_3(X_1,0,X_3,t) &= -i\omega \tilde{u}_3(k_\parallel \omega | X_3) e^{ik_\parallel X_1} e^{-i\omega t}, \end{aligned} \tag{25}$$

with $\boldsymbol{v_1} = \mathrm{Re}\{\tilde{\boldsymbol{v}}_1\}$.

Equation (23) may be written in complex notation as

$$-\boldsymbol{F} = \rho_0 \cdot \frac{1}{2} \mathrm{Re} \begin{pmatrix} 2\tilde{v}_1 \dfrac{\partial \tilde{v}_1^*}{\partial X_1} + \left(\tilde{v}_3 \dfrac{\partial \tilde{v}_1^*}{\partial X_3} + \tilde{v}_1 \dfrac{\partial \tilde{v}_3^*}{\partial X_3} \right) \\ 0 \\ 2\tilde{v}_3 \dfrac{\partial \tilde{v}_3^*}{\partial X_3} + \left(\tilde{v}_3 \dfrac{\partial \tilde{v}_1^*}{\partial X_1} + \tilde{v}_1 \dfrac{\partial \tilde{v}_3^*}{\partial X_1} \right) \end{pmatrix} \tag{26}$$

where the superscript* stands for the complex conjugate quantity.

Upon insertion of Eq. (25) in Eq. (26) the nonzero components of the acoustic streaming force may be expressed in terms of the displacement field

$$\begin{cases} F_1 = -\rho_0 \omega^2 e^{-2k_\parallel'' X_1} \left(-k_\parallel'' \overline{u}_1 \overline{u}_1^* + \dfrac{1}{2} \mathrm{Re} \left[\overline{u}_3 \dfrac{\partial \overline{u}_1^*}{\partial X_3} + \overline{u}_1 \dfrac{\partial \overline{u}_3^*}{\partial X_3} \right] \right) \\ F_3 = -\rho_0 \omega^2 e^{-2k_\parallel'' X_1} \left(-k_\parallel'' \, \mathrm{Re}[\overline{u}_1 \overline{u}_3^*] + \mathrm{Re} \left[\overline{u}_3 \dfrac{\partial \overline{u}_3^*}{\partial X_3} \right] \right). \end{cases} \tag{27}$$

In Eq. (27) $\overline{u}$ denotes in short $\tilde{u}(k_\parallel \omega | X_3)$ and $k_\parallel''$ is the imaginary part of the modulus of the complex wave vector $\boldsymbol{k}_\parallel (k_\parallel = k_\parallel' + ik_\parallel'')$. The relations in Eq. (27) provide a simple mean of calculating the acoustic streaming force from the knowledge of the first-order acoustic displacement field.

E. Second-order acoustic forces on deposited particle

During megasonic cleaning, a contaminant solid particle adhering to the surface of a wafer may be removed if it is subjected to a force counteracting the adhesion force. Since

the attractive adhesion force is perpendicular to the silicon/water interface and oriented toward the solid, the removal force also has to be normal to the surface but directed in the opposite direction. Considering the effect of the second-order sound field on particle removal, only the component of the streaming force F_3 may give rise to such a removal force. Here, we also make the assumption that the solid particle does not alter the first-order sound field. This approximation is justified since the contaminant particles we are considering have diameters on the order of 1 μm or smaller, and that the wavelength of the incident acoustic wave is on the order of a millimeter.

The net force due to the second-order sound field acting on a particle subjected to the time-independent second-order pressure field p_2 is

$$\boldsymbol{f}=\int_S p_2 \boldsymbol{n} dS, \tag{28}$$

where the integral is over the surface of the particle and $\boldsymbol{n}$ is the normal to that surface. Upon conversion of the surface integral into a volume integral, the second-order net force becomes

$$\boldsymbol{f}=\int_V \nabla p_2 dV. \tag{29}$$

We insert Eq. (22) into Eq. (29) to obtain

$$\boldsymbol{f}=\int_V (\boldsymbol{F}+\mu\nabla^2 \boldsymbol{v}_2) dV. \tag{30}$$

The silicon/water interface prevents the fluid from flowing in directions parallel to the axis X_3, and the component of the streaming velocity in that direction is zero. The removal force may then be defined as the third component of the second-order force f_3 via

$$f_3=\int_V F_3 dV. \tag{31}$$

In order to calculate the removal force it is therefore only necessary to determine the component of the streaming force perpendicular to the wafer/water interface.

The first component of the second-order force f_1 cannot be calculated from the streaming force F_1 since in that direction the fluid is set in motion and we do not know the streaming velocity, $\boldsymbol{v_2}$ [see Eq. (30)]. We anticipate however, that a strong F_1 will result in large streaming velocities near the silicon/water interface and therefore strong drag forces on contaminant particles in that direction. We therefore associate qualitatively in the rest of the article, a large F_1 to large forces that may pull/push or roll contaminant particles adhering to the wafer surface.

III. RESULTS

A. Silicon/water system

Let us illustrate the procedure for obtaining the displacement field in an inhomogeneous medium composed of two semi-infinite media separated by a single planar interface subjected to an incident acoustic wave. We locate the interface at $X_3=0$ and denote by (1) the medium to the left of the interface (silicon) and by (2) the water to the right of the interface. We assume that the incident wave is launched in the liquid [medium (2)] toward the silicon/water interface. The components of the displacement of the bulk wave is given in a two dimensional Fourier space parallel to the $X_3=0$ plane in the form[13]

$$\begin{aligned}
\tilde{U}_1(k_\parallel \omega | X_3) &= \frac{B}{Z} e^{\alpha_l^{(2)} X_3}, \\
\tilde{U}_2(k_\parallel \omega | X_3) &= 0, \\
\tilde{U}_3(k_\parallel \omega | X_3) &= -i \frac{\alpha_l^{(2)}}{k_\parallel} \frac{B}{Z} e^{\alpha_l^{(2)} X_3},
\end{aligned} \tag{32}$$

where B is the wave amplitude and $i=\sqrt{-1}$. Z is a normalizing factor equal to $\sqrt{1-(\alpha_l^{(2)}/k_\parallel)^2}$ and $\alpha_l^{(2)}$ is given in appendix.

The wave vector $k_\parallel$ of a bulk compressive (longitudinal) incident plane wave is related to the incidence angle θ the incoming wave makes with the normal to the interface, by the relation

$$k_\parallel = \frac{\omega}{C_{l(2)}} \sin\theta. \tag{33}$$

The inverse of the Green's function, $\overleftrightarrow{g}_s^{-1}$ of a semi-infinite medium ''i'', bounded by a free surface at $X_3=0$, is given in the appendix as Eq. (A3). The inverse of the surface Green's functions of the two semi-infinite media are inserted into Eq. (18) to obtain the inverse of the surface Green's function of the solid/fluid inhomogeneous medium

$$\overleftrightarrow{g}^{-1}(k_\parallel \omega | 0,0) = \overleftrightarrow{g}_{s1}^{-1}(k_\parallel \omega | 0,0) + \overleftrightarrow{g}_{s2}^{-1}(k_\parallel \omega | 0,0). \tag{34}$$

The matrix $\overleftrightarrow{g}^{-1}(k_\parallel \omega | 0,0)$ is then inverted to obtain $\overleftrightarrow{g}(k_\parallel \omega | 0,0)$.

The inverse of the Green's function is inserted in Eq. (20) to calculate the variation in density of vibrational states of the silicon/water interface. For this we have used the following data: a silicon density of 2.33×10^3 kg/m^3, a density of water of 10^3 kg/m^3, longitudinal speed of sound in water of 1500 m/s, and transverse and longitudinal speed of sound in silicon of 5843 and 8433 m/s, respectively. The coefficient of dilatation viscosity μ' is chosen to be one third of the coefficient of shear viscosity, μ with $\mu=10^{-3}$ Pa s^{-1}. We have calculated the variation in density of state of the silicon/water system according to Eq. (20) using a reference composed of one half of an infinite silicon medium and one half of an infinite water medium. Figure 2 reports on that variation in density of states as a function of pulsation at some given $k_\parallel$. For computational convenience, we have chosen a real valued $k_\parallel$ because of the small magnitude of its imaginary part relative to its real part due to the low viscosity of water. This figure shows several interesting features. The feature around a pulsation of 1 Mrad/s corresponds to the lower bound of the bulk vibrational band of the fluid. However, a refinement of the density of states in this vicinity (see

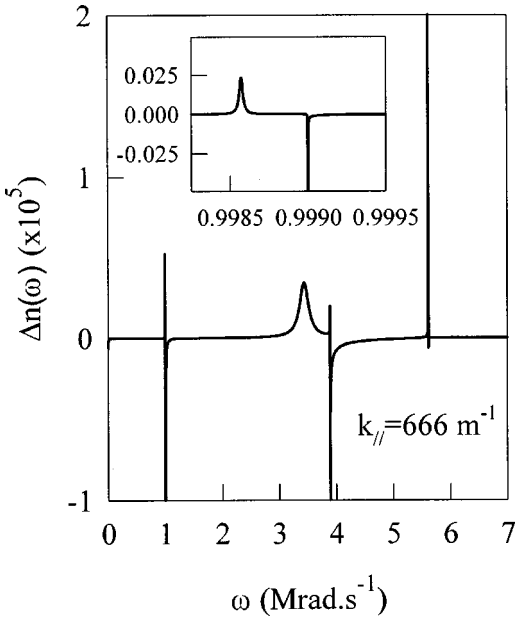

FIG. 2. Variation in density of vibrational states as a function of pulsation for the system containing a single silicon/water interface. The inset is a magnification of the plot around the lower limit of the water bulk band below which the Stoneley–Scholte mode exists. The wave vector of the incident wave is constant and takes the value indicated on the graph.

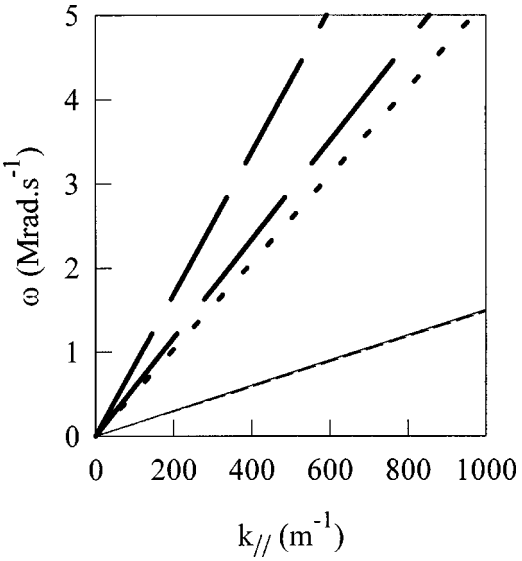

FIG. 3. Dispersion curves for the system with a single silicon/water interface. The thin solid line is the dispersion curve for the fluid. The thin dashed line indicates the dispersion relation for the Stoneley–Scholte mode. The long-dash lines refer to the dispersion curves for the transverse (lower curve) and longitudinal (upper curve) waves. The dotted line represents the pulsation/wave vector relationship for the Rayleigh wave.

inset) indicates the presence of a peak below the bulk band of the fluid. This peak represents a Stoneley–Scholte surface wave localized in the liquid at the fluid/solid interface. A localized Stoneley–Scholte wave propagates in the fluid in a direction parallel to the solid/fluid interface. Its amplitude decays exponentially with distance from the solid/fluid interface. However, since the Stoneley–Scholte wave lies below the bulk band of the liquid it cannot be excited by an incident bulk wave originating from the liquid, such as one produced by the transducer in the megasonic tank. The sharp features near 3.9 and 5.6 Mrad/s are the lower limits of the transverse and longitudinal vibrational bulk bands of silicon. A broader peak located at 3.4 Mrad/s and below the bulk band of silicon is associated with a Rayleigh wave localized at the surface of the solid. This is a wave that propagates in the solid in a direction parallel to the interface which amplitude decreases exponentially inside the solid. The acoustic band structure of the silicon/water system is then reported in Fig. 3. In this figure, we plot pulsation versus the wave vector. From our calculations we find that the dispersions relation for the Rayleigh and Stoneley–Scholte waves are given as $\omega = 5157 k_{\parallel}$ and $1499.36 k_{\parallel}$, respectively.

The elastic displacement field in the fluid region (2) of the inhomogeneous system is derived from Eq. (19),

$$\begin{aligned}\tilde{\boldsymbol{u}}(k_{\parallel}\omega|X_3) = {} & \tilde{\boldsymbol{U}}(k_{\parallel}\omega|X_3) \\ & - \overleftrightarrow{G}_2(k_{\parallel}\omega|X_3,0)\overleftrightarrow{G}_2^{-1}(k_{\parallel}\omega|0,0)\tilde{\boldsymbol{U}}(k_{\parallel}\omega|0) \\ & + \overleftrightarrow{G}_2(k_{\parallel}\omega|X_3,0)\overleftrightarrow{G}_2^{-1}(k_{\parallel}\omega|0,0)\overrightarrow{g}(k_{\parallel}\omega|0,0) \\ & \times \overleftrightarrow{G}_2^{-1}(k_{\parallel}\omega|0,0)\tilde{\boldsymbol{U}}(k_{\parallel}\omega|0), \end{aligned} \tag{35}$$

where $\overleftrightarrow{G}_2(k_{\parallel}\omega|X_3,X_3')$ is given in the appendix by replacing the appropriate elastic coefficients with those of Eq. (15).

After lengthy algebraic manipulations, the components of the elastic displacement field in the water are obtained as

$$\begin{aligned}\tilde{u}_1(k_{\parallel}\omega|X_3)\frac{Z}{B} &= e^{\alpha_l^{(2)}X_3} + \xi_r e^{-\alpha_l^{(2)}X_3} + \xi_t e^{-\alpha_t^{(2)}X_3}, \\ \tilde{u}_2(k_{\parallel}\omega|X_3) &= 0, \\ \tilde{u}_3(k_{\parallel}\omega|X_3)\frac{Z}{B} &= -i\frac{\alpha_l^{(2)}}{k_{\parallel}}\left[e^{\alpha_l^{(2)}X_3} - \xi_r e^{-\alpha_l^{(2)}X_3} - \frac{\xi_t}{\epsilon^{(2)}}e^{-\alpha_t^{(2)}X_3}\right], \end{aligned} \tag{36}$$

where

$$\begin{aligned}\xi_r = {} & -\frac{1+\epsilon^{(2)}}{1-\epsilon^{(2)}} + \frac{2}{A}\frac{2\rho^{(2)}\epsilon^{(2)}}{(1-\epsilon^{(2)})^2}\omega^2\psi_2 \\ & + \frac{1}{A}\frac{2\rho^{(2)}}{(1-\epsilon^{(2)})^2}\frac{\omega^4}{k_{\parallel}^4}[\alpha_l^{(2)}\psi_1 + \alpha_t^{(2)}\epsilon^{(2)}\psi_3] \\ \xi_t = {} & 2\frac{\epsilon^{(2)}}{1-\epsilon^{(2)}} - \frac{1}{A}\frac{2\rho^{(2)}(1+\epsilon^{(2)})\epsilon^{(2)}}{(1-\epsilon^{(2)})^2}\omega^2\psi_2 \\ & - \frac{1}{A}\frac{2\rho^{(2)}\epsilon^{(2)}}{(1-\epsilon^{(2)})^2}\frac{\omega^4}{k_{\parallel}^4}[\alpha_l^{(2)}\psi_1 + \alpha_t^{(2)}\psi_3] \end{aligned} \tag{37}$$

with

$$\psi_1=\frac{\rho^{(1)}\alpha_t^{(1)}}{1-\epsilon^{(1)}}+\frac{\rho^{(2)}\alpha_t^{(2)}}{1-\epsilon^{(2)}},$$

$$\psi_2=\rho^{(1)}\left[-2C_{t(1)}^2+\frac{\omega^2}{k_\parallel^2(1-\epsilon^{(1)})}\right]-\rho^{(2)}\times\left[-2C_{t(2)}^2+\frac{\omega^2}{k_\parallel^2(1-\epsilon^{(2)})}\right], \tag{38}$$

$$\psi_3=\frac{\rho^{(1)}\alpha_l^{(1)}}{1-\epsilon^{(1)}}+\frac{\rho^{(2)}\alpha_l^{(2)}}{1-\epsilon^{(2)}},$$

and

$$A=\frac{\omega^4}{k_\parallel^4}\psi_1\psi_3-k_\parallel^2\psi_2^2. \tag{39}$$

All other quantities have been defined previously.

We combine Eq. (36), (37), (38), (39), and (27) to calculate the components of the streaming force. As a check for our method, we have verified, in the limit of a rigid solid/water interface and an incident plane wave parallel to the interface, that the component F_1 of the streaming force takes the same analytical form as that reported by Nyborg.[12] It is also easy to verify analytically that in the case of a nonviscous fluid, the component $F_1=0$ since the conditions of continuity of the displacements at the solid/liquid interface does not have to be satisfied in the direction X_1, that is, the fluid may slide freely on the solid.

We calculate numerically the components of the streaming force near the silicon/water interface in the case of traveling plane waves in the fluid and as a function of incidence angle of the incoming wave (see Fig. 4). This force is calculated at 0.1 μm from the interface and at a frequency typically used in megasonic cleaning of 700 kHz (ω=4.398 Mrad/s). Again for the sake of simplicity in this calculation, we use a real $k_\parallel$ defined as $k_\parallel=(\omega/C)\sin\theta$. The components of the streaming force along the interface F_1 is one to two orders of magnitude larger than F_3. The streaming force does not vary significantly and remains small outside a narrow range of angles centered on the value corresponding to the excitation of the Rayleigh wave. The sign of F_3 changes drastically across the conditions for stimulating the Rayleigh wave. A positive F_3 gives rise to a removal force opposing the adhesion force acting on some contaminant particle. Adhesion is promoted by a negative F_3. In Fig. 5, we present F_3 as a function of X_3 in the vicinity of the silicon/water interface for two different conditions. These correspond to modes of vibration that can be excited by incident traveling plane waves, namely a plane wave grazing the interface exciting a fluid bulk mode [Fig. 5(a)] and a plane wave at an angle of 16.57° from the normal to the interface that stimulates the Rayleigh wave [Fig. 5(b)]. In the two cases, the acoustic boundary layer where the sound field is controlled by the continuity condition of the solid and fluid displacements at the interface extends only over a very few micrometers owing to the low viscosity of water. An increase in shear viscosity has, for effect, to extend the acoustic boundary layer. The thickness of the acoustic boundary layer scales as $\sqrt{\mu/\omega\rho}$. Incident waves grazing the silicon/water interface

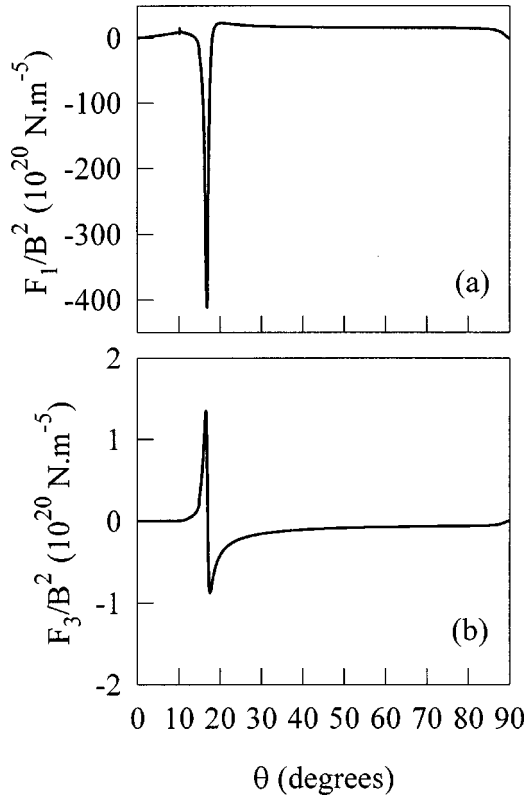

FIG. 4. Components of the streaming force parallel (a) and perpendicular (b) to the silicon/water interface as functions of the angle the incident wave makes with the normal to the interface. The streaming force is normalized to the square of the displacement amplitude of the incident wave *B*. The streaming force is calculated at a distance of 0.1 μm from the interface. The pulsation has the value 4.398 Mrad/s.

[see Fig. 5(a)], as is the case in a typical megasonic cleaning tank, produce an extremely small streaming force F_3. The streaming force is essentially negligible outside the acoustic boundary layer. In contrast, the magnitude of F_3 is increased manyfold by choosing an angle of incidence that satisfies the dispersion relation for the Rayleigh wave [see Fig. 5(b)]. The force appears to be constant beyond a few micrometers, however, at large distances, extending over hundreds of micrometers, from the silicon/water interface, F_3 varies periodically with X_3 according to the factor $\sin 2\alpha_l^{(2)''}X_3$ where $\alpha_l^{(2)''}$ is the imaginary part of the complex number $\alpha_l^{(2)}$. The very small value of water's coefficient of shear viscosity makes F_1 and F_3 almost independent of X_1 over distances on the order of millimeters.

In summary, excitation of the Rayleigh wave seems to be the most favorable case for contaminant particle removal from a single silicon/water interface.

B. Water/silicon/water system

We model a silicon wafer by a slab of solid medium 1 of thickness d which surfaces are perpendicular to the axis X_3 and located at $X_3=\pm d/2$ [see Fig. 1(b)]. The inverse Green's function of the slab in the space of its surfaces is reported in the appendix [Eq. (A5)]. The silicon slab is coupled on its two sides to two semi-infinite media. The semi-infinite media are constituted of water (medium 2) and the inverse Green's function at their respective surface is

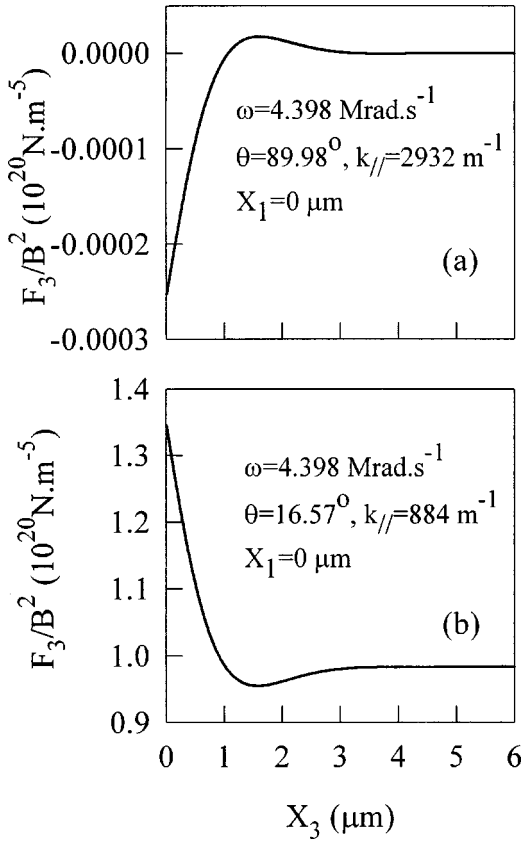

FIG. 5. Normal component of the streaming force as a function of distance from the silicon/water interface in the case of (a) a nearly grazing incident plane wave and (b) the Rayleigh wave.

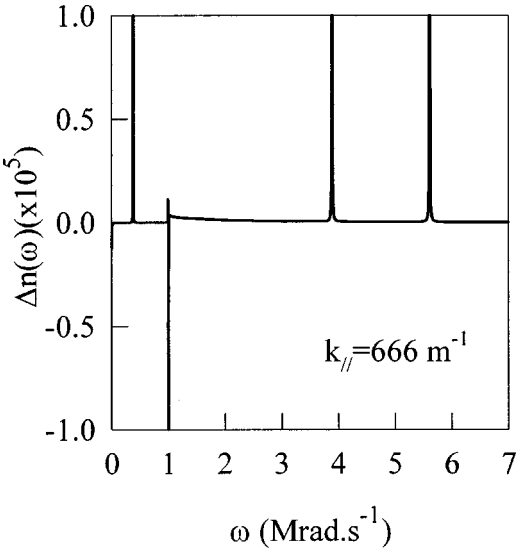

FIG. 6. Variation in density of vibrational states as a function of pulsation for the system composed of a silicon slab (wafer) immersed in water. The wave vector of the incident wave is constant and takes the value indicated on the graph.

obtained from Eq. (A3). The inverse of the Green's function of a silicon slab immersed in water, defined at the solid/fluid interfaces is then obtained from Eq. (18). The variation in density of vibrational states of this inhomogeneous medium is then determined numerically from Eq. (20) using an infinite water medium as reference system. We have taken a silicon slab of thickness $d=0.64$ mm as representative of a standard wafer. The speed of sound and coefficient of viscosity are the same as in Sec. III A. Figure 6 reports on the variation in density of states as a function of pulsation for the same real $k_{\|}$ used in the case of a single solid/water interface. The feature near 1 Mrad/s is again the lower limit of the bulk band of the fluid. The bulk band of the solid does not appear in this figure since the slab has finite dimensions along the axis X_3. A finite slab possesses only discrete vibrational states that become resonant states when coupled to semi-infinite fluid media. The resonant states show as sharp peaks in the density of states within the bulk band of the fluid. We note that the pulsation at which these resonances occur corresponds to those of the lower bound of the transverse and longitudinal bulk bands of silicon. Finally, Δn exhibits a well-defined peak below the lower limit of the bulk band of water, for ω around 0.33 MHz. This peak is associated with the first flexural mode of vibration of the slab.[14] The flexural modes of higher order are not observed since their frequencies exceed those considered in this study. The first order flexural mode is localized within the fluid near the silicon wafer/water interface. This mode being localized in the liquid at the interface between a solid and a liquid, we will refer subsequently to this flexural mode as a wave of the Stoneley–Scholte type. Again, this surface wave cannot be excited by an incident plane wave launched from the liquid. We have verified that as the thickness of the slab increases, the number of resonant peaks and the pulsation of the Stoneley–Scholte wave increase. In the limit of an infinitely thick slab, one recovers the result of Fig. 2, that is, the resonant states merge into a solid band, the pulsation of the Stoneley–Scholte wave approaches that of the bulk band of the liquid and a peak corresponding to the Rayleigh wave forms below the transverse bulk band of the solid. We have calculated the variation in density of states for several values of the wave vector, $k_{\|}$. Figure 7 represents the dispersion relations $\omega(k_{\|})$ for the Stoneley–Scholte wave, the bulk band of the fluid as well as the resonant states in the solid. The density of states calculated with the IRT includes all possible modes of vibration of the water/silicon/water system, including flexural modes of the wafer. However, in the case of a silicon wafer with a thickness of $d=0.64$ mm, the resonances associated with the flexural modes are unobservable in the range of frequencies and wave vectors ($k_{\|}$) considered. Indeed, in the long wavelength limit ($k_{\|}d \ll 1$) considered in this study, the lowest localized mode which corresponds to the first flexural mode (referred to as Stoneley–Scholte wave), cannot be excited by an incoming wave from the liquid, whereas the next flexural modes are situated at frequencies well above the frequency domain considered.

To calculate the first-order acoustic displacement field in the fluid near the slab, we insert into Eq. (19), the inverse of $\overleftrightarrow{g}^{-1}(MM)$ along with the Green's function of bulk water and the displacement of an incident wave with the form given by Eq. (30). The first-order displacement field is then used to determine the components of the second-order streaming force according to Eq. (27). The two components

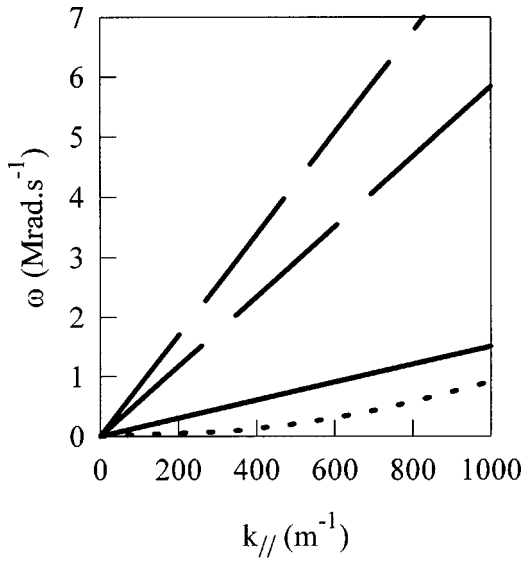

FIG. 7. Dispersion curves for the water/silicon/water system. The dispersion curves for the solid are represented by the long-dash lines. The continuous line refers to the dispersion curve of the fluid. The dotted line corresponds to the pulsation/wave vector relationship for a Stoneley–Scholte wave localized in the liquid at the solid/fluid interface.

of the streaming force at a fixed location from the $X_3 = +d/2$ slab/water interface as a function of incidence angle are reported in Fig. 8. Here, we consider an incident plane wave originating in the fluid of pulsation 4.398 Mrad/s.

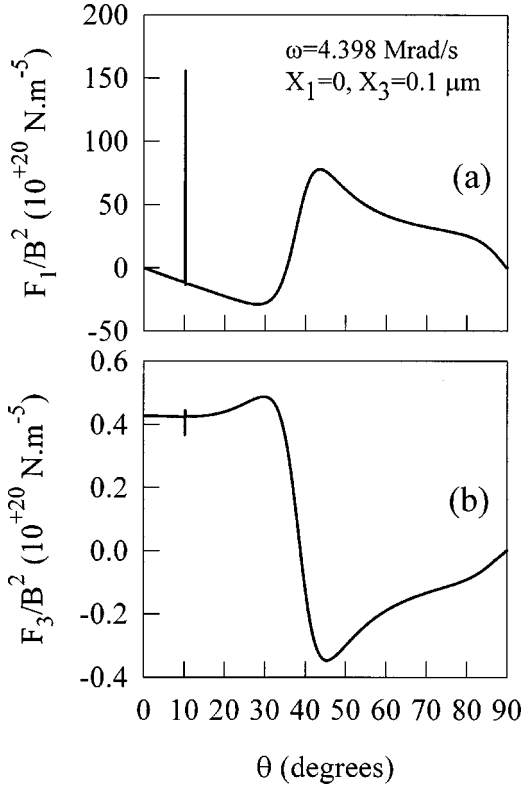

FIG. 8. Components of the streaming force parallel (a) and perpendicular (b) to one of the silicon/water interfaces in the water/silicon/water system as functions of the angle the incident wave makes with the normal to the interface. The streaming force is normalized to the square of the displacement amplitude of the incident wave *B*. The streaming force is calculated at a distance of 0.1 μm from the interface.

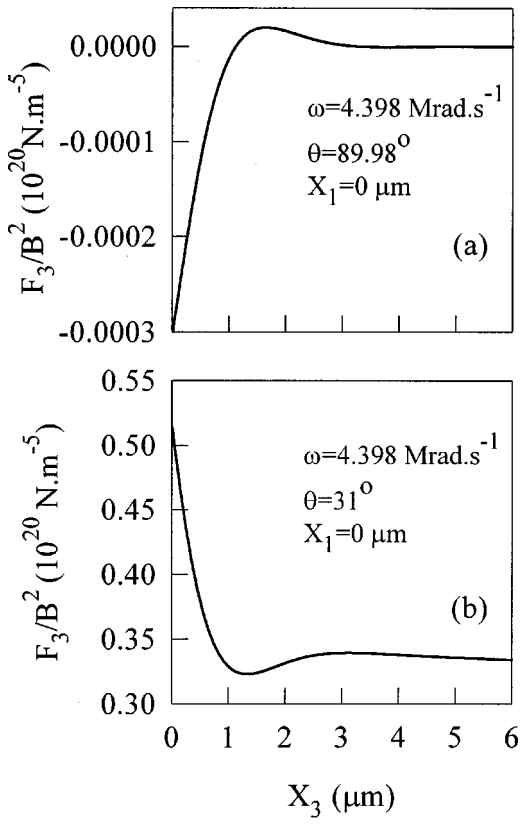

FIG. 9. Normal component of the streaming force as a function of distance from one silicon/water interface in the case of incident waves with incident angles equal to (a) ~90° and (b) 31°. The system is composed of a silicon slab immersed in water.

Again the component of the force F_1 exceeds F_3 by up to two orders of magnitude. F_1 shows a sharp increase at an angle of incidence ~10° (or $k_{\|} \sim 500\,\mathrm{m}^{-1}$) corresponding to the resonant state associated with the longitudinal mode of the solid.

Finally, we illustrate the variation of F_3 and F_1 with distance from the slab/water interface in Figs. 9 and 10 for incident waves with two different incidence angles, namely a grazing plane wave [Figs. 9(a) and 10(a)] and a plane wave with an incidence of 31° [Figs. 9(b) and 10(b)]. In all cases, owing to the small viscosity of water, the acoustic boundary layer does not exceed 3 μm. The acoustic streaming force perpendicular to the wafer/water interface is negligibly small in the case of a grazing incident wave [Fig. 9(a)]. On the other hand, at an optimum incidence of 31° [Fig. 9(b)], a significant positive force exists inside the fluid extending over a wide range of distances from the interface. The streaming force parallel to the silicon/water interface F_1 shows similar behaviors although it exceeds the force F_3 by one to two orders of magnitude. Beyond the distances reported in Figs. 9 and 10, F_1 and F_3 vary sinusoidally in a manner similar to the case of a single solid/water interface.

IV. COMPARISON BETWEEN SECOND-ORDER ACOUSTIC FORCES AND PARTICLE ADHESION FORCE

To calculate removal forces, we consider two particular cases. The first case is that of the silicon/water system with

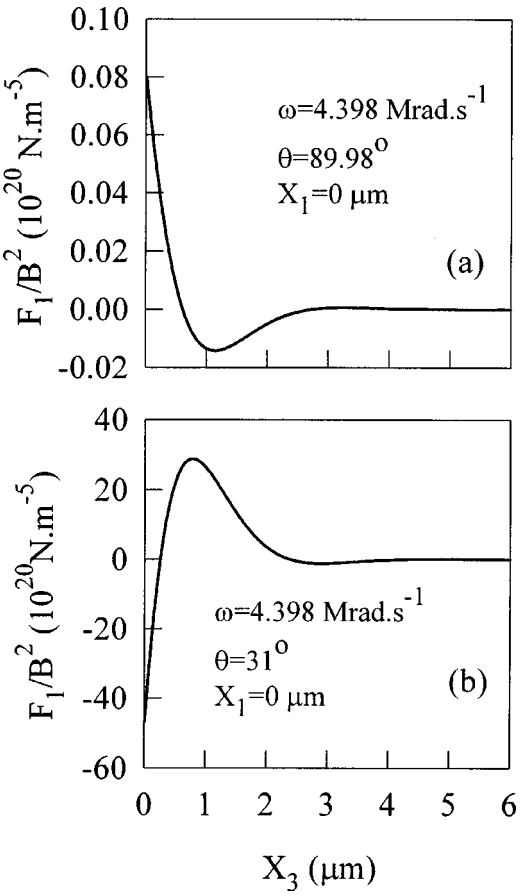

FIG. 10. Component of the streaming force parallel to the silicon/water interface as a function of distance from one silicon/water interface in the case of incident waves with incident angles equal to (a) ~90° and (b) 31°. The system is composed of a silicon slab immersed in water.

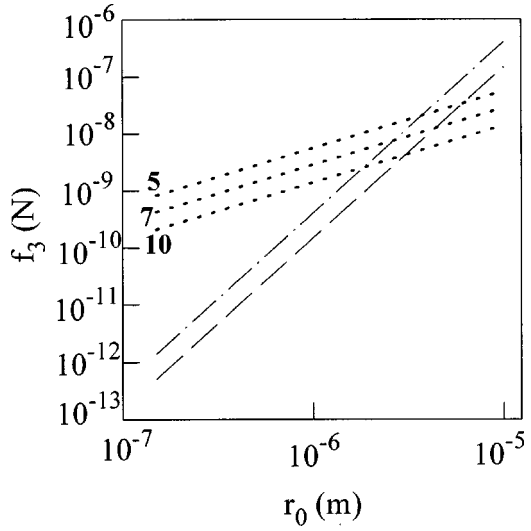

FIG. 11. Removal and adhesion forces on a spherical particle adhering to the silicon surface as a function of particle radius. The adhesion forces represented as dotted lines are for three different separation distances between the particle and the silicon surface, namely 5, 7, and 10 Å. The dashed-dotted line stands for the removal force in the case of the silicon/water system for an excited Rayleigh wave. The dashed line refers to the water/silicon/water system and excitation of a bulk wave [see Fig. 9(b) for details].

an incident plane wave of pulsation $\omega=4.398$ Mrad/s ($\nu=700$ kHz) and an incident angle $\theta=16.57°$. These conditions correspond to the excitation of the Rayleigh wave. For the purpose of estimating the removal force, we neglect the variation of F_3 within the acoustic boundary layer and assume that it takes its minimum value of $F_3/B^2 \approx 0.96 \times 10^{20}\,\mathrm{N/m^5}$ for all X_3's [see Fig. 5(b)]. In this case the removal force given by Eq. (31) takes the simpler form $f_3 = 0.96 \times 10^{20} B^2 V$ where V is the volume of the particle. For a spherical particle of radius r_0, $V = \frac{4}{3}\pi r_0^3$, the removal force scales as the cube of the radius of the particle. In addition, it varies as the square of the incident wave's displacement amplitude. For megasonic transducers and typical megasonic cleaning conditions, the displacement amplitude is on the order of 1×10^{-6} m.[15]

The second case, investigated here, corresponds to a silicon wafer immersed in water (water/silicon/water system) with a pulsation $\omega=4.398$ Mrad/s ($\nu=700$ kHz) and an incident angle $\theta=31°$. Again for the sake of simplicity, the variation of F_3 with distance as illustrated in Fig. 9 is neglected and we take $F_3/B^2 \approx 0.32 \times 10^{20}\,\mathrm{N/m^5}$ for all X_3's. With this, the removal force acting on a spherical particle is given by the simple relation: $f_3 = 0.32 \times 10^{20} B^2 \frac{4}{3}\pi r_0^3$.

The London–van der Waals adhesion force is usually considered to be the dominant force for short distances in particle adhesion.[6] The van der Waals force of adhesion between a spherical particle and a planar surface is given by[16]

$$f_{vdW} = \frac{A_{132} r_0}{6(X_3 - r_0)^2}, \tag{40}$$

where X_3 is the distance of the center of the particle to the surface. The effective Hamaker constant A_{132} is a function of the material constituting the particle (material 1), the surface (material 2), and the medium surrounding the particle/surface system (material 3). Here, we consider the case of a silica contaminant particle in water adhering to a wafer coated with a thin layer of silica. Since the silica layer on the wafer surface is extremely thin compared to the wavelength of the acoustic waves considered here, it will not affect the results for the streaming force. The Hamaker constant for that system is $A_{132} = 0.83 \times 10^{-20}$ J.[17,18] In the case of a particle nearly in contact with the surface, the separation distance, $X_3 - r_0$, is only on the order of a few angstroms.[19] We select three values: $X_3 - r_0 = 5$, 7, 10 Å as a representative set of separation distances.

In Fig. 11, we report on the variation with particle radius of the removal forces due to a Rayleigh wave at a solid/fluid interface, a bulk wave for a wafer in water as well as van der Waals adhesive forces.

The removal forces associated with the Rayleigh and bulk wave cross the adhesive forces at radii exceeding several micrometers. The second-order streaming force F_3 is therefore only capable of removing large contaminant particles from silicon wafers. However, for small particles, the adhesive force dominates and the component of the removal force perpendicular to the solid/fluid interface is not sufficient to remove particles. We note, though, that the streaming force along the solid/fluid interface was several orders of

magnitude larger than the component along X_3. This streaming force may then serve as a mechanism for wafer cleaning by rolling and tugging the particles along its surface. The contaminant particles will be removed from the wafer surface when they reach the edge of the wafer. The direction of motion of the contaminant particle along the wafer is determined by the sign of F_1.

V. CONCLUSIONS

We have calculated the first-order acoustic field in the case of a single interface between silicon and water and a silicon slab immersed in water. The solid was treated as an isotropic elastic medium and water as a viscous fluid. The first-order acoustic field was then used to determine the second-order streaming force that allows us to estimate the removal force that acts on a spherical contaminant particle adhering to the solid surface. The removal force was then compared to the van der Waals adhesion force between a silica particle and a flat silicon surface in water. We found that in general the removal force resulting from the second-order acoustic field is too small to remove submicron particle. However, the component of the streaming force parallel to the solid/fluid interface F_1 is orders of magnitude larger than the component F_3. In this case, F_1 may lead to particle removal by a rolling and tugging mechanism as suggested by some authors.[20] In the literature on megasonic cleaning it has been customary to compare the magnitude of the force acting on the contaminant particle along the silicon/water interface to the adhesion force.[6] This practice does not reflect the fact that these two forces have directions perpendicular to each other. There is no resisting force to the motion of the particle in the direction parallel to the silicon/water interface but a friction force at the particle/silicon interface. The fluid flow in the direction X_1 due to the streaming force F_1 will lead to a drag force that may push a contaminant particle or roll it depending on the magnitude of the friction force. A detailed study of this mechanism will be the subject of a subsequent publication. Finally, we have shown that subjecting a silicon wafer to a grazing incident acoustic wave as is traditionally done in megasonic cleaning tanks may not lead to an optimum cleaning efficiency. Indeed we have shown that the normal and parallel components of the streaming force are strongly dependent on the incidence angle of the incoming wave. Our results suggest that cleaning efficiency may be improved by subjecting a wafer to incident acoustic waves sampling a wide range of incidence angles. We recall that excitation of the longitudinal resonant mode of the wafer at an incidence of 10° (frequency of 700 kHz) yields a very strong positive streaming force F_1. These results further support the recently developed high-efficiency single-wafer megasonic cleaning technology using a cylindrical quartz crystal positioned parallel to the top surface of a wafer that generates acoustic waves with variable incidence angles.[21] With this technology the surface of a silicon wafer is stimulated by megasonic waves with incidence angle varying between approximately $-45°$ and 45°.

ACKNOWLEDGMENTS

This research was supported in part by a grant from the Center for Microcontamination Control at the University of Arizona. One of us (P. A. D.) would like to acknowledge the financial support of the ''Laboratoire de Dynamique et Structures des Matériaux Moléculaires'', U. F. R. de Physique, Université de Lille I, France, where some of this work was done.

APPENDIX

The nonzero elements of the Green's function of a bulk (solid or liquid) homogeneous medium, $\overleftrightarrow{G}(k_\parallel \omega | X_3, X_3')$, solution of Eq. (9), are given by[22]

$$
\begin{aligned}
G_{11} &= -\frac{k_\parallel^2}{2\rho\alpha_l\omega^2}\left[e^{-\alpha_l|X_3-X_3'|} - \epsilon e^{-\alpha_t|X_3-X_3'|}\right],\\
G_{13} &= G_{31} = \frac{ik_\parallel}{2\rho\omega^2}\,\mathrm{sgn}(X_3-X_3')\\
&\quad\times\left[e^{-\alpha_t|X_3-X_3'|} - e^{-\alpha_l|X_3-X_3'|}\right],\\
G_{33} &= -\frac{k_\parallel^2}{2\rho\alpha_t\omega^2}\left[-\epsilon e^{-\alpha_l|X_3-X_3'|} + e^{-\alpha_t|X_3-X_3'|}\right],\\
G_{22} &= -\frac{1}{2\rho\alpha_t C_t^2}\,e^{-\alpha_t|X_3-X_3'|},
\end{aligned}
\tag{A1}
$$

where we have defined

$$
\begin{aligned}
\alpha_l^2 &= k_\parallel^2 - \frac{\omega^2}{C_l^2},\\
\alpha_t^2 &= k_\parallel^2 - \frac{\omega^2}{C_t^2},\\
\epsilon &= \frac{\alpha_t\alpha_l}{k_\parallel^2}.
\end{aligned}
\tag{A2}
$$

α_l and α_t are defined with the following sign convention:[21]

$$
\alpha_{l,t} = \sqrt{k_\parallel^2 - \frac{\omega^2}{C_{l,t}^2}} \quad \text{if } \omega \leqslant k_\parallel C_{l,t}
$$

$$
\alpha_{l,t} = -i\sqrt{\frac{\omega^2}{C_{l,t}^2} - k_\parallel^2} \quad \text{if } \omega \geqslant k_\parallel C_{l,t}.
$$

The inverse of the Green's function, $\overleftrightarrow{g}_s^{-1}$ of a semi-infinite medium *i*, bounded by a free surface at $X_3 = 0$, is given in the domain of its surface by[13]

$$g_{si}^{-1}(k_{\|}\omega|X_3=0,X_3'=0)=\begin{pmatrix} -\dfrac{\alpha_l^{(i)}\omega^2\rho^{(i)}}{k_{\|}^2(1-\epsilon^{(i)})} & 0 & \pm i\rho^{(i)}k_{\|}\left[-2C_{t(i)}^2+\dfrac{\omega^2}{k_{\|}^2(1-\epsilon^{(i)})}\right] \\ 0 & -\rho^{(i)}\alpha_t^{(i)}C_{t(i)}^2 & 0 \\ \mp i\rho^{(i)}k_{\|}\left[-2C_{t(i)}^2+\dfrac{\omega^2}{k_{\|}^2(1-\epsilon^{(i)})}\right] & 0 & -\dfrac{\alpha_t^{(i)}\omega^2\rho^{(i)}}{k_{\|}^2(1-\epsilon^{(i)})} \end{pmatrix} \tag{A3}$$

where the signs $\pm$ (and $\mp$) are used for semi-infinite media located at $X_3\leqslant 0(+)$ and $X_3\geqslant 0(-)$, respectively.

We consider a slab of silicon (medium 1) of thickness d which surfaces are perpendicular to the axis X_3 and located at $X_3=\pm d/2$. The inverse Green's function of the slab in the space of its surfaces has been derived previously[23] and is given by

$$\overleftrightarrow{g}_{s1}^{-1}(MM)=\begin{pmatrix} \overleftrightarrow{g}_{s1}^{-1}\left(k_{\|}\omega\middle|-\frac{d}{2},-\frac{d}{2}\right) & \overleftrightarrow{g}_{s1}^{-1}\left(k_{\|}\omega\middle|-\frac{d}{2},+\frac{d}{2}\right) \\ \overleftrightarrow{g}_{s1}^{-1}\left(k_{\|}\omega\middle|+\frac{d}{2},-\frac{d}{2}\right) & \overleftrightarrow{g}_{s1}^{-1}\left(k_{\|}\omega\middle|+\frac{d}{2},+\frac{d}{2}\right) \end{pmatrix} \tag{A4}$$

which components take the analytical form

$$\overleftrightarrow{g}_{s1}^{-1}(MM)=\begin{pmatrix} \alpha_1 & 0 & iq_1 & h_1 & 0 & if_1 \\ 0 & v_1 & 0 & 0 & w_1 & 0 \\ -iq_1 & 0 & b_1 & if_1 & 0 & e_1 \\ h_1 & 0 & -if_1 & a_1 & 0 & -iq_1 \\ 0 & w_1 & 0 & 0 & v_1 & 0 \\ -if_1 & 0 & e_1 & iq_1 & 0 & b_1 \end{pmatrix}, \tag{A5}$$

with

$$a_1=\frac{H_1\alpha_l^{(1)}\omega^2}{2k_{\|}C_{t(1)}^2}[sh(\alpha_t^{(1)}d)ch(a_l^{(1)}d)-\epsilon^{(1)}sh(\alpha_l^{(1)}d)ch(\alpha_t^{(1)}d)],$$

$$b_1=\frac{H_1\alpha_t^{(1)}\omega^2}{2k_{\|}C_{t(1)}^2}[sh(\alpha_l^{(1)}d)ch(\alpha_t^{(1)}d)-\epsilon^{(1)}sh(\alpha_t^{(1)}d)ch(\alpha_l^{(1)}d)],$$

$$q_1=H_1\left\{\epsilon^{(1)}(3k_{\|}^2+\alpha_t^{(1)2})\left[sh^2\left(\alpha_l^{(1)}\frac{d}{2}\right)ch^2\left(\alpha_t^{(1)}\frac{d}{2}\right)+sh^2\left(\alpha_t^{(1)}\frac{d}{2}\right)ch^2\left(\alpha_l^{(1)}\frac{d}{2}\right)\right]-\frac{1}{2}[2\alpha_l^{(1)}\alpha_t^{(1)}\epsilon^{(1)}+(\alpha_t^{(1)2}+k_{\|}^2)]\right.$$
$$\left.sh(\alpha_t^{(1)}d)sh(\alpha_l^{(1)}d)\right\},$$

$$h_1=-\frac{H_1\alpha_l^{(1)}\omega^2}{2k_{\|}C_{t(1)}^2}[sh(\alpha_t^{(1)}d)-\epsilon^{(1)}sh(\alpha_l^{(1)}d)],$$

$$e_1=-\frac{H_1\alpha_t^{(1)}\omega^2}{2k_{\|}C_{t(1)}^2}[sh(\alpha_l^{(1)}d)-\epsilon^{(1)}sh(\alpha_t^{(1)}d)], \tag{A6}$$

$$f_1=-H_1\epsilon^{(1)}\frac{\omega^2}{C_{t(1)}^2}\left[sh^2\left(\alpha_l^{(1)}\frac{d}{2}\right)-sh^2\left(\alpha_t^{(1)}\frac{d}{2}\right)\right],$$

$$H_1=-\frac{\rho^{(1)}C_{t(1)}^2}{2k_{\|}}\left[ch\left(\alpha_l^{(1)}\frac{d}{2}\right)sh\left(\alpha_t^{(1)}\frac{d}{2}\right)-\epsilon^{(1)}ch\left(\alpha_t^{(1)}\frac{d}{2}\right)sh\left(\alpha_l^{(1)}\frac{d}{2}\right)\right]^{-1}\times\left[sh\left(\alpha_l^{(1)}\frac{d}{2}\right)ch\left(\alpha_t^{(1)}\frac{d}{2}\right)-\epsilon^{(1)}sh\left(\alpha_t^{(1)}\frac{d}{2}\right)ch\left(\alpha_l^{(1)}\frac{d}{2}\right)\right]^{-1},$$

$$v_1=-\rho^{(1)}\alpha_t^{(1)}C_{t(1)}^2\frac{ch(\alpha_t^{(1)}d)}{sh(\alpha_t^{(1)}d)},$$

$$w_1=-\rho^{(1)}\alpha_t^{(1)}C_{t(1)}^2\frac{(-1)}{sh(\alpha_t^{(1)}d)}.$$

In Eq. (A4), the dependency on frequency and wave vector is implicit.

[1] M. Olim, J. Electrochem. Soc. **144**, 3657 (1997).
[2] Y. Wu, Ph.D. dissertation, University of Minnesota, 1997.
[3] P. A. Deymier, A. Khelif, J. O. Vasseur, B. Djafari-Rouhani, and S. Raghavan, J. Appl. Phys. **88**, 2423 (2000).
[4] S. Schwatzman, A. Mayer, and W. Kern, RCA Rev. **46**, 81 (1985).
[5] R. Gouk, Master thesis, University of Minnesota, 1996.
[6] D. Zhang, Ph.D. dissertation, University of Minnesota, 1993.
[7] C. Eckart, Phys. Rev. **73**, 68 (1948).
[8] H. Schlichting, *Boundary-Layer Theory*, 6th Ed. (McGraw-Hill, New York, 1968).
[9] S. A. Elder, J. Acoust. Soc. Am. **31**, 56 (1959).
[10] T. Ohmi *et al.*, Mater. Res. Soc. Symp. Proc. **477**, 6 (1997).
[11] L. Dobrzynski, Surf. Sci. **180**, 489 (1987).
[12] W. L. Nyborg, in *Acoustic Streaming, Physical Acoustics*, edited by W. P. Mason (Academic, London, 1965), Vol. II B, Chap. 11.
[13] L. Dobrzynski, Surf. Sci. Rep. **11**, 139 (1990).
[14] I. A. Viktorov, *Rayleigh and Lamb Waves: Physical Theory and Applications* (Plenum, New York, 1967).
[15] In *Handbook of Semiconductor Cleaning Technology*, edited by W. Kern (Noyes, Park Ridge, NJ, 1993).

[16] M. B. Renade, Aerosol. Sci. Technol. **7**, 161 (1987).
[17] J. Visser, Adv. Colloid Interface Sci. **3**, 331 (1972).
[18] J. Israelachvilii, *Intermolecular and Surface Forces*, 2nd ed. (Academic, San Diego, 1994).
[19] W. C. Hinds, *Aerosol Technology* (Wiley, New York, 1982).
[20] S. Middelman and A. K. Hockberg, *Process Engineering Analysis in Semiconductor Device Fabrication* (McGraw-Hill, New York, 1993).
[21] G. Willits and B. Fraser, *Semiconductor Fabtech*, 10th ed. (ICG Publishing, London, 1999).
[22] A. A. Maradudin and D. L. Mills, Ann. Phys. **100**, 262 (1976).
[23] L. Dobrzynski, J. Mendialdua, A. Rodriguez, S. Bolibo, and M. More, J. Phys. (France) **50**, 2563 (1989).